ELSEVIER

0141-1187(94)00016-6

Applied Ocean Research 17 (1995) 21–32
Elsevier Science Limited
Printed in Great Britain

Hopf bifurcations and nonlinear studies of gain margins in path control of marine vehicles

Fotis A. Papoulias & Zeki Okan Oral

Department of Mechanical Engineering, Naval Postgraduate School, Monterey, CA 93943, USA

(Received 21 July 1993; accepted 28 June 1994)

The problem of loss of stability of marine vehicles under cross-track error control in the presence of a mathematical model versus actual system mismatch is analyzed. Emphasis is placed on studying the response of the system after the initial loss of stability of straight line motion. Center manifold reduction and integral averaging methods are used in order to study bifurcations to periodic solutions and stability of the resulting limit cycles. Numerical integrations are used to confirm the theoretical results and to establish regions of asymptotic stability. The methods used in this work demonstrate the significance of nonlinear terms in assessing the response of the system.

NOMENCLATURE

a	Linear yaw rate coefficient in first order model
a_3	Cubic yaw rate coefficient in first order model
A	Closed loop dynamics matrix for the linearized system
b	Rudder angle coefficient in first order model
C	Heading angle, yaw rate, or position error gain factor
C_ψ	Critical value of heading angle gain factor
C_r	Critical value of yaw rate gain factor
C_y	Critical value of position error gain factor
ITAE	Integral of Time Absolute Error, $\int_0^\infty t\|e\|\,dt$ criterion
I_z	Vehicle mass moment of inertia
k_ψ	Heading angle gain
k_r	Yaw rate gain
k_y	Position error gain
$\mathcal{K}$	Cubic stability coefficient
m	Vehicle mass
N_i	Derivative of yaw moment N with respect to the indicated variable
NPS	Naval Postgraduate School
PAH	Poincaré–Andronov–Hopf bifurcation
r	Yaw rate
R	Polar coordinate of transformed reduced system
t	Time
T	Limit cycle period
T	Matrix of eigenvectors of **A**
v	Sway velocity
x	State variable vector
y	Deviation off the commanded path
Y_i	Derivative of sway force Y with respect to the indicated variable
z	State variables vector in canonical form
z_1, z_2	Critical variables of **z**
z_3	Stable coordinate of **z**
δ	Rudder angle deflection
δ_0	Linear feedback rudder control law
δ_{sat}	Saturation value of δ
ψ	Vehicle heading angle
ω_n	Natural frequency of the ITAE control law

1 INTRODUCTION

Accurate path control of surface ships and underwater vehicles along prescribed geographical paths is a fundamental problem which is becoming increasingly important, particularly as the missions of ocean vehicles become more sophisticated with strict requirements for performance. In order for a control law to be able to perform its mission in a realistic operational scenario it has to be robust enough so that it can maintain a stability and accuracy of operations in the presence of modeling errors and environmental uncertainties. The robustness properties of the design are particularly important due to the unpredictable nature of the ocean environment and the changes in the hydrodynamic characteristics of the vehicle during turning, changes in the forward speed, or operations in proximity to other objects in the area. For these reasons, there exists a need for the analysis of the robustness characteristics of a

particular control law design and the establishment of a rational operational envelope based on stability and performance criteria. Previous studies[1] showed that gain adaptation is highly desirable due to changes in the linearized vehicle hydrodynamics with different operating conditions, such as depth under keel. The resulting adaptation scheme[2] required significant vehicle motion which may be undesirable when operating in restricted waters, or during object recognition and localization tasks. Integral control techniques[3] proved quite effective, but neglected the nonlinear behavior of the vehicle which becomes very important at low speeds and hover operations. Model based compensators exhibit robust behavior under conditions of parameter uncertainty which is as good as the classical linear quadratic regulators for linear output feedback systems.[4] Alternatively, sliding mode controllers exhibit very robust characteristics given an estimate of the parameter uncertainty and/or disturbances.[5,6] Sliding mode control, however, does not offer an infinitely robust design and it suffers from a series of bifurcation phenomena and loss of stability unless proper care is exercised.[7]

In this work the authors analyze the problem of the loss of stability of a path keeping control law under conditions far from nominal. We assume that the autopilot has been designed based on a nominal model, whereas the actual system is different. For demonstration purposes we employ a linear full state feedback control law, but the methods are quite general and can be used for other designs as well. The main loss of stability cases analyzed here occurs in the form of generic bifurcations to periodic solutions.[8] We use center manifold reduction techniques and averaging in order to capture the stability properties of the resulting limit cycles.[9] Particular emphasis is placed on the control gains as the primary bifurcation parameters, since they are related to gain margins in linear control theory.[10] It is shown that the classical definition of the gain margin which does not take into consideration the influence of nonlinear terms, can lead to inaccurate predictions with regards to practical system stability. Extensive use is made of numerical integrations in order to confirm the theoretical results. All computations in this work are conducted for the NPS autonomous underwater vehicle[11] and all results are presented in standard dimensionless quantities with respect to the vehicle length, 7·3 ft, and nominal forward speed, 2 ft/s.

2 PROBLEM FORMULATION

2.1 Equations of motion

The linear maneuvering equations of motion of a marine vehicle in the horizontal plane are written in dimensionless form as,

$$m(\dot{v} + r + x_G\dot{r}) = Y_{\dot{r}}\dot{r} + Y_{\dot{v}}\dot{v} + Y_r r + Y_v v + Y_\delta \delta \tag{1}$$

$$I_z\dot{r} + mx_G(\dot{v} + r) = N_{\dot{r}}\dot{r} + N_{\dot{v}}\dot{v} + N_r r + N_v v + N_\delta \delta \tag{2}$$

where standard notation is used and all symbols are explained in the Nomenclature. Equations (1) and (2) can be used to derive a second order transfer function between the rudder angle δ and yaw rate r. The fundamental dynamics of turning are captured by a simpler version, where a first order lag exists between δ and r,

$$\dot{r} = ar + b\delta \tag{3}$$

Equation (3), which is sometimes referred to as Nomoto's first order model,[12] is particularly useful in control system design since no sway velocity feedback is necessary. For small unmanned vehicles where the available space is a minimum, this is important since it eliminates the need for side slip angle sensors. Typical dimensionless values for a and b for the NPS vehicle are $a = -1{\cdot}47$ and $b = -2{\cdot}86$. Equation (3) predicts the linear variation of the steady state turning rate versus rudder angle. In reality, the r–δ curve has the characteristics of a softening spring mainly due to speed loss during turning. To account for this, a modified version of (3) is used, namely

$$\dot{r} = ar + a_3 r^3 + b\delta \tag{4}$$

where a_3 is usually determined from steady state results. Typical r–δ curves for the NPS AUV are shown in Fig. 1. The nominal value of a_3 is taken to be $-1{\cdot}0$ in this work, although its actual value varies considerably in practice due to a variety of unmodeled dynamics and changes in the vehicle characteristics. Finally, the model is completed by the incorporation of the kinematic equations,

$$\dot{\psi} = r \tag{5}$$

$$\dot{y} = \sin\psi \tag{6}$$

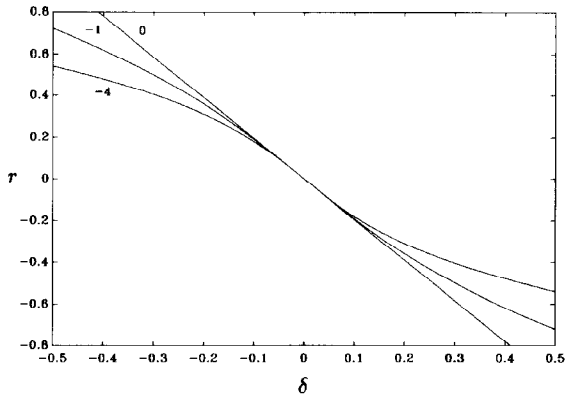

Fig. 1. Steady state r–δ curves for different values of a_3.

where ψ is the vehicle heading, and y the cross-track error off a desired straight line path.

2.2 Control law

A linear full state feedback control law is based on the linearized version of eqns (3), (5) and (6) around the nominal state $\psi = r = y = 0$,

$$\begin{aligned} \dot{\psi} &= r \\ \dot{r} &= ar + b\delta_0 \\ \dot{y} &= \psi \end{aligned} \tag{7}$$

where δ_0 is the feedback rudder angle for small deviations of ψ, r, y from the nominal,

$$\delta_0 = k_\psi \psi + k_r r + k_y y \tag{8}$$

The closed loop characteristic equation is obtained from (7) and (8),

$$\lambda^3 - (a + bk_r)\lambda^2 - bk_\psi \lambda - bk_y = 0 \tag{9}$$

If the desired characteristic equation has the general form

$$\lambda^3 + \alpha_2 \lambda^2 + \alpha_1 \lambda + \alpha_0 = 0 \tag{10}$$

the control gains are computed from,

$$\begin{aligned} k_\psi &= -\frac{\alpha_1}{b} \\ k_r &= -\frac{\alpha_2 + a}{b} \\ k_y &= -\frac{\alpha_0}{b} \end{aligned} \tag{11}$$

The coefficients α_0, α_1, α_2 can be tuned so that the closed loop system has the desired dynamics. For demonstration purposes, eqn (10) is tuned to the ITAE optimal form for third order systems,

$$\alpha_0 = \omega_n^3, \qquad \alpha_1 = 2{\cdot}15\omega_n^2, \qquad \alpha_2 = 1{\cdot}75\omega_n \tag{12}$$

The natural frequency ω_n can be selected according to the desired controller bandwidth.[10] Higher values of ω_n correspond to a more responsive control law and increased rudder activity. In order to capture the effect of rudder saturation, the commanded rudder angle is given by

$$\delta = \delta_{sat} \tanh\left(\frac{\delta_0}{\delta_{sat}}\right) \tag{13}$$

where δ_0 is the slope of δ at the origin given by (8), and δ_{sat} is the saturation limit on δ typically set at 0·4 radians. The hyperbolic tangent function (13) is used instead of a hard saturation function because of its analyticity properties. As we will see in the following sections, the slope δ_0 and the limit δ_{sat} are much more important than the actual functional form utilized to model saturation effects.

2.3 Loss of stability

The previously defined control law will guarantee stability and performance provided the vehicle modeling properties are accurately known. An important quantity in assessing the robustness of a particular control law design to parameter variations and unmodeled dynamics is the gain margin. This is defined as the extent to which changes can be inflicted on the system gain without loss in stability. To this end, it is assumed that the heading error gain k_ψ is multiplied by a constant C. In order to compute the critical value of C for the stability of straight line motion,

$$\delta = Ck_\psi \psi + k_r r + k_y y$$

is substituted into (7) and the characteristic equation obtained

$$\lambda^3 - (a + bk_r)\lambda^2 - Cbk_\psi \lambda - bk_y = 0$$

Loss of stability occurs when the Routh–Hurwitz criterion is violated,

$$(a + bk_r)Cbk_\psi = -bk_y$$

and using (11) this yields the critical value of C for stability,

$$C_\psi = \frac{\alpha_0}{\alpha_1 \alpha_2} \tag{14}$$

or, using (12),

$$C_\psi = 0{\cdot}2658 \tag{15}$$

Stability is lost when C becomes less than C_ψ. Using similar calculations for the yaw rate gain k_r, one can find,

$$C_r = \frac{\alpha_0 + \alpha_1 a}{\alpha_1(\alpha_2 + a)} = \frac{\omega_n + 2{\cdot}15a}{2{\cdot}15(1{\cdot}75\omega_n + a)} \tag{16}$$

As shown in Fig. 2, the system is stable for $C < C_r$ when $\omega_n < -a/1{\cdot}75$, and for $C > C_r$ when $\omega_n > -a/1{\cdot}75$. Finally, the corresponding calculations for the positional error gain k_y, yield

$$C_y = \frac{\alpha_1 \alpha_2}{\alpha_0} = 3{\cdot}7625 \tag{17}$$

and the system remains stable for $C < C_y$.

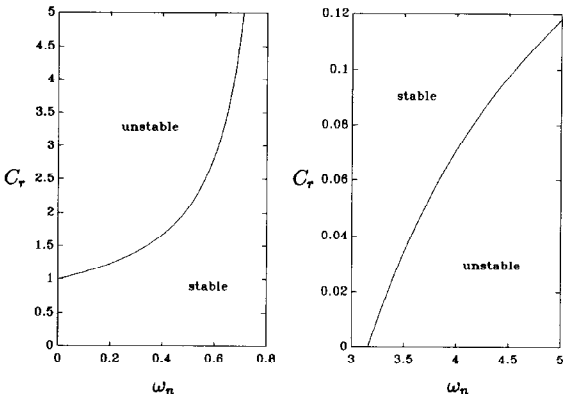

Fig. 2. Critical value C_r versus ω_n.

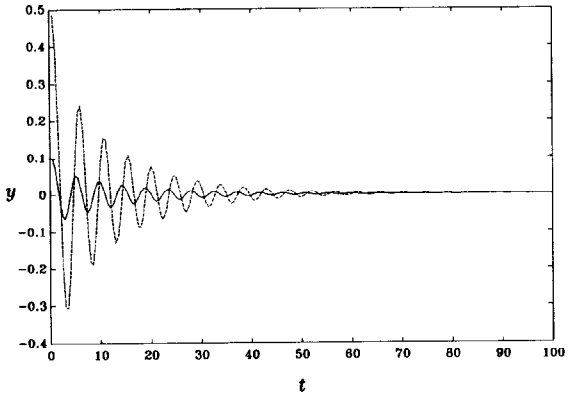

Fig. 3. Time history (t, y) for $\omega_n = 1{\cdot}0$ and $C = 0{\cdot}8C_y$.

As the coefficient C crosses its critical value, C_ψ, C_r, or C_y, one pair of complex conjugate roots of the corresponding characteristic equation of the linearized system crosses the imaginary axis transversally. This is known as a generic Poincaré–Andronov–Hopf (PAH) bifurcation,[8] and a family of periodic solutions coexists locally with the stable/unstable nominal equilibrium state.

The bifurcation point is easily computed with linear methods, as above. However, two equally important questions remain to be answered, namely,

- do periodic solutions exist before or after the bifurcation parameter crosses its critical point, and
- are the resulting limit cycles stable or unstable?

To address these issues, one has to isolate and study the effect of the dominant nonlinear terms in the equations of motion. As a motivation for this study, the problem is first demonstrated through a series of numerical integrations. Figures 3 and 4 present simulation results in terms of the lateral offset y versus time t for the case $C = 0{\cdot}8C_y$. According to the stability analysis results, this corresponds to stable straight line motion. The simulations are performed for different initial conditions in y, and the natural frequency ω_n is selected at 1·0 for Fig. 3 and 2·0 for Fig. 4, respectively. Although the linearized stability results do not distinguish between different values of ω_n, an important qualitative change in the simulation results is observed. For $\omega_n = 1{\cdot}0$ it appears that solutions converge to the nominal path regardless of the initial disturbance. On the other hand, for $\omega_n = 2{\cdot}0$ convergence is guaranteed only for initial disturbances that are small enough. If this is not the case, it appears that the solutions are attracted by a stable limit cycle. The nonlinear techniques employed in the following section should be able to predict and explain these two phenomena.

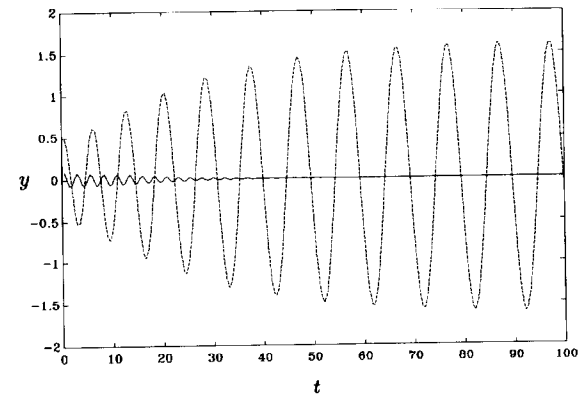

Fig. 4. Time history (t, y) for $\omega_n = 2{\cdot}0$ and $C = 0{\cdot}8C_y$.

3 HOPF BIFURCATIONS

3.1 Normal form computation

The complete system is given by

$$\begin{aligned} \dot{\psi} &= r \\ \dot{r} &= ar + a_3 r^3 + b\delta_{sat} \tanh\left[\frac{1}{\delta_{sat}}(Ck_\psi \psi + k_r r + k_y y)\right] \\ \dot{y} &= \sin\psi \end{aligned} \tag{18}$$

or, in compact form,

$$\dot{\mathbf{x}} = \mathbf{f}(\mathbf{x}), \qquad \mathbf{x} = [\psi, r, y]^T \tag{19}$$

where the analysis focuses on the heading error gain factor. System (19) is written in the form,

$$\dot{\mathbf{x}} = \mathbf{A}\mathbf{x} + \mathbf{g}(\mathbf{x}) \tag{20}$$

where $\mathbf{A}$ is the Jacobian matrix of $\mathbf{f}(\mathbf{x})$ evaluated at $\mathbf{x} = \mathbf{0}$, and $\mathbf{g}(\mathbf{x})$ contains all nonlinear terms of eqns (18). Expanding $\mathbf{g}(\mathbf{x})$ in Taylor series and keeping the first nonvanishing coefficients only, the following is obtained

$$\dot{\mathbf{x}} = \mathbf{A}\mathbf{x} + \mathbf{g}^{(3)}(\mathbf{x}) \tag{21}$$

where $\mathbf{g}^{(3)}(\mathbf{x})$ contains third order terms,

$$\begin{aligned} g_1^{(3)} &= 0 \\ g_2^{(3)} &= -\frac{b}{3\delta_{sat}^2}\delta_0^3 \\ g_3^{(3)} &= -\tfrac{1}{6}\psi^3 \end{aligned} \tag{22}$$

The δ_0^3 term in (22) can be easily computed in terms of the gains k_ψ, k_r, k_y, and the factor C.

At the bifurcation point, $C = C_\psi$, matrix $\mathbf{A}$ has the eigenvalues

$$\lambda_1 = \sqrt{\frac{\alpha_0}{\alpha_2}}\,i, \qquad \lambda_2 = -\sqrt{\frac{\alpha_0}{\alpha_2}}\,i, \qquad \lambda_3 = -\alpha_2 \tag{23}$$

If we introduce the transformation matrix,

$$\mathbf{T} = \begin{bmatrix} 1 & 0 & 1 \\ 0 & -\sqrt{\alpha_0/\alpha_2} & -\alpha_2 \\ 0 & \sqrt{\alpha_2/\alpha_0} & -1/\alpha_2 \end{bmatrix}$$

the linear change of coordinates,

$$\mathbf{x} = \mathbf{T}\mathbf{z}\,, \quad \mathbf{z} = \mathbf{T}^{-1}\mathbf{x} \tag{24}$$

transforms system (21) into its normal form,

$$\dot{\mathbf{z}} = \mathbf{T}^{-1}\mathbf{A}\mathbf{T}\mathbf{z} + \mathbf{T}^{-1}\mathbf{g}^{(3)}\mathbf{T}\mathbf{z} \tag{25}$$

Equation (24) can be used to obtain the relationships between the physical variables ψ, r, y and the transformed variables,

$$\begin{aligned} \psi &= z_1 + z_3 \\ r &= -\sqrt{\frac{\alpha_0}{\alpha_2}}z_2 - \alpha_2 z_3 \\ y &= \sqrt{\frac{\alpha_2}{\alpha_0}}z_2 - \frac{1}{\alpha_2}z_3 \end{aligned} \tag{26}$$

Coordinate z_3 corresponds to the negative eigenvalue λ_3 in (23) and is, therefore, asymptotically stable. The PAH bifurcations are localized on the center manifold of (20), a two dimensional surface that is locally approximated by the Euclidean plane spanned by the eigenvectors of **A** which correspond to the purely imaginary eigenvalues λ_1 and λ_2. Center manifold theory[8] establishes that the stable coordinate z_3 can be expressed as a function of the critical coordinates z_1, z_2, and this relationship is at least of quadratic order. In fact, due to the symmetry of the problem, $z_3 = \mathcal{O}(z_1^3, z_2^3)$. Therefore, z_3 has zero contributions to the third order expansions in (25), and one can approximate (26) by,

$$\psi = z_1\,, \qquad r = -\sqrt{\frac{\alpha_0}{\alpha_2}}z_2\,, \qquad y = \sqrt{\frac{\alpha_2}{\alpha_0}}z_2 \tag{27}$$

Substitution of (27) into (25) yields,

$$\dot{z}_1 = -\sqrt{\frac{\alpha_0}{\alpha_2}}z_2 + r_{11}z_1^3 + r_{12}z_1^2 z_2 + r_{13}z_1 z_2^2 + r_{14}z_2^3 \tag{28}$$

$$\dot{z}_2 = \sqrt{\frac{\alpha_0}{\alpha_2}}z_1 + r_{21}z_1^3 + r_{22}z_1^2 z_2 + r_2 z_1 z_2^2 + r_{24}z_2^3 \tag{29}$$

where the terms r_{ij} are evaluated from (22) and (27) at the bifurcation point C_ψ.

For values of C close to its critical value, eqns (28) and (29) become,

$$\begin{aligned} \dot{z}_1 = {} & \alpha'\varepsilon z_1 - \left(\sqrt{\frac{\alpha_0}{\alpha_2}} + \omega'\varepsilon\right)z_2 + r_{11}z_1^3 + r_{12}z_1^2 z_2 \\ & + r_{13}z_1 z_2^2 + r_{14}z_2^3 \end{aligned} \tag{30}$$

$$\begin{aligned} \dot{z}_2 = {} & \left(\sqrt{\frac{\alpha_0}{\alpha_2}} + \omega'\varepsilon\right)z_1 + \alpha'\varepsilon z_2 + r_{21}z_1^3 + r_{22}z_1^2 z_2 \\ & + r_2 z_1 z_2^2 + r_{24}z_2^3 \end{aligned} \tag{31}$$

where ε is the difference between C and C_ψ,

$$C = C_\psi + \varepsilon = \frac{\alpha_0}{\alpha_1\alpha_2} + \varepsilon \tag{32}$$

The terms α' and ω' denote the derivative of the real and imaginary part, respectively, of the critical pair of eigenvalues λ_1, λ_2 with respect to C evaluated at C_ψ. These can be computed using a regular perturbation series approach,[13] as follows. The characteristic equation of the linearized system matrix **A** is

$$\lambda^3 + \alpha_2\lambda^2 + \left(\frac{\alpha_0}{\alpha_2} + \alpha_1\varepsilon\right)\lambda + \alpha_0 = 0 \tag{33}$$

The complex conjugate eigenvalues are expressed as

$$\lambda_{1,2} = \alpha'\varepsilon \mp \left(\sqrt{\frac{\alpha_0}{\alpha_2}} + \omega'\varepsilon\right)i \tag{34}$$

If (34) is substituted into (33) and terms of order ε^2 or higher are neglected, one gets

$$\alpha' = -\frac{\alpha_2^2\alpha_1}{2(\alpha_0 + \alpha_2^3)}\,, \qquad \omega' = \frac{\alpha_2\alpha_1}{2(\alpha_0 + \alpha_2^3)}\sqrt{\frac{\alpha_0}{\alpha_2}} \tag{35}$$

The third order terms in (30) and (31) remain the same as in (28) and (29). These are evaluated for $\varepsilon = 0$ since additional terms of the form εz_i^3 are higher order compared to z_i^3 and can be neglected.

3.2 Integral averaging

Writing eqns (30) and (31) in the form,

$$\dot{z}_1 = \alpha'\varepsilon z_1 - (\omega_0 + \omega'\varepsilon)z_2 + F_1(z_1, z_2) \tag{36}$$

$$\dot{z}_2 = (\omega_0 + \omega'\varepsilon)z_1 + \alpha'\varepsilon z_2 + F_2(z_1, z_2) \tag{37}$$

where $\omega_0 = \sqrt{\alpha_0/\alpha_2}$, if polar coordinates are introduced as

$$z_1 = R\cos\theta\,, \quad z_2 = R\sin\theta \tag{38}$$

eqns (36) and (37) result in

$$\dot{R} = \alpha'\varepsilon R + F_1(R,\theta)\cos\theta + F_2(R,\theta)\sin\theta \tag{39}$$

$$R\dot{\theta} = (\omega_0 + \omega'\varepsilon)R + F_2(R,\theta)\cos\theta - F_1(R,\theta)\sin\theta \tag{40}$$

Equation (39) yields

$$\dot{R} = \alpha'\varepsilon R + \mathcal{P}(\theta)R^3 \tag{41}$$

where $\mathcal{P}(\theta)$ is a 2π-periodic function in the angular coordinate θ. If (41) is averaged over one cycle in θ,[9] one gets an equation with constant coefficients,

$$\dot{R} = \alpha'\varepsilon R + \mathcal{K}R^3 \tag{42}$$

where

$$\mathcal{K} = \frac{1}{2\pi}\int_0^{2\pi}\mathcal{P}(\theta)\,\mathrm{d}\theta \tag{43}$$

Carrying out the indicated integration in (43) results in,

$$\mathcal{K} = \frac{\alpha_2^3 + \alpha_0}{8\alpha_2}\left[3a_3 - \frac{\alpha_2^2}{2\alpha_0} + \frac{1}{b^2\delta_{\text{sat}}^2}(\alpha_2 + a)\left(\frac{\alpha_0}{\alpha_2} + a^2\right)\right] \tag{44}$$

Similar averaging is performed for eqn (40), which is written as

$$\dot{\theta} = \omega_0 + \omega'\varepsilon + \mathcal{M}R^2 \tag{45}$$

where

$$\mathcal{M} = \frac{1}{8}(3r_{21} + r_{23} - r_{12} - 3r_{14}) \tag{46}$$

and the coefficients r_{ij} are given by,

$$r_{21} = -(\alpha_2^3 + \alpha_0)\left(\frac{\alpha_0^{3/2}}{3b^2\delta_{sat}^2\alpha_2^{5/2}} + \frac{\alpha_2^{5/2}}{6\alpha_0^{3/2}}\right)$$

$$r_{23} = -\frac{\alpha_0^{1/2}}{\alpha_2^{3/2}}(\alpha_2^3 + \alpha_0)\frac{a^2}{b^2\delta_{sat}^2}$$

$$r_{12} = -\left(\frac{\alpha_0}{\alpha_2}\right)^{1/2}(\alpha_2^3 + \alpha_0)\frac{a}{b^2\delta_{sat}^2}$$

$$r_{14} = -\left(\frac{\alpha_2}{\alpha_0}\right)(\alpha_2^3 + \alpha_0)\left(a_3 + \frac{a^3}{3b^2\delta_{sat}^2}\right)$$

The existence and stability of limit cycles can be determined by analyzing the equilibrium points of the averaged equation (42), which correspond to periodic solutions in z_1, z_2 as can be seen from (38). From eqn (42) it can easily be seen that:

1. If $\alpha' > 0$, then
   (a) if $\mathcal{K} > 0$, unstable periodic solutions coexist with the stable equilibrium for $\varepsilon < 0$, and
   (b) if $\mathcal{K} < 0$, stable periodic solutions coexist with the unstable equilibrium for $\varepsilon > 0$.
2. If $\alpha' < 0$, then
   (a) if $\mathcal{K} > 0$, unstable periodic solutions coexist with the stable equilibrium for $\varepsilon > 0$, and
   (b) if $\mathcal{K} < 0$, stable periodic solutions coexist with the unstable equilibrium for $\varepsilon < 0$.

We refer to $\mathcal{K} < 0$ as the *supercritical*, and $\mathcal{K} > 0$ as the *subcritical* PAH bifurcation. In the supercritical case, after the equilibrium state loses its stability the system converges to a stable periodic solution with an amplitude which increases continuously as the difference ε is increased. In the subcritical case, however, before the equilibrium state loses stability, its domain of attraction becomes very small since it is bounded by the amplitudes of the unstable limit cycles. In such a case, an initial disturbance of sufficient magnitude can throw the system off the nominal path even before its domain of attraction has completely shrunk to zero. As the nominal equilibrium becomes unstable, the system jumps to a different state of motion with a locally, at $\varepsilon = 0$, discontinuous increase in the amplitude.

For the case of yaw rate gain variation, similar calculations yield,

$$\psi = z_1\,, \quad r = -\sqrt{\alpha_1}z_2\,, \quad y = \frac{1}{\sqrt{\alpha_2}}z_2\,, \quad \omega_0 = \sqrt{\alpha_1}$$

$$\alpha' = -\frac{\alpha_1^3(\alpha_2 + a)}{2(\alpha_1^3 + \alpha_0^2)}\,, \qquad \omega' = -\frac{\alpha_0\alpha_1^{3/2}(\alpha_2 + a)}{2(\alpha_1^3 + \alpha_0^2)}$$

$$\mathcal{K} = \frac{1}{8}(3r_{11} + r_{13} + r_{22} + 3r_{24})$$

$$\mathcal{M} = \frac{1}{8}(3r_{21} + r_{23} - r_{12} - 3r_{14})$$

where

$$r_{11} = \frac{\alpha_0\alpha_1^2}{\alpha_0^2 + \alpha_1^3}\left(\frac{\alpha_1^2}{3b^2\delta_{sat}^2} - \frac{1}{6}\right)\,, \quad r_{13} = \frac{a^2}{b^2\delta_{sat}^2}\cdot\frac{\alpha_0\alpha_1^3}{\alpha_0^2 + \alpha_1^3}$$

$$r_{22} = \frac{a}{b^2\delta_{sat}^2}\cdot\frac{\alpha_1^5}{\alpha_0^2 + \alpha_1^3}\,,$$

$$r_{24} = \frac{\alpha_1^4}{\alpha_0^2 + \alpha_1^3}\cdot\left(a_3 + \frac{a^3}{3b^2\delta_{sat}^2}\right)$$

$$r_{21} = -\frac{1}{\alpha_0^2 + \alpha_1^3}\left(\frac{\alpha_1^{11/2}}{3b^2\delta_{sat}^2} + \frac{\alpha_0^2\alpha_1^{1/2}}{6}\right)$$

$$r_{23} = -\frac{a^2}{b^2\delta_{sat}^2}\cdot\frac{\alpha_1^{9/2}}{\alpha_0^2 + \alpha_1^3}\,, \qquad r_{12} = -\frac{a}{b^2\delta_{sat}^2}\cdot\frac{\alpha_0\alpha_1^{7/2}}{\alpha_0^2 + \alpha_1^3}$$

$$r_{14} = -\frac{\alpha_0\alpha_1^{5/2}}{\alpha_0^2 + \alpha_1^3}\left(\frac{a^3}{3b^2\delta_{sat}^2} + a_3\right)$$

Finally, for the case of the positional error gain variation,

$$\psi = z_1\,, \quad r = -\sqrt{\alpha_1}z_2\,, \quad y = \frac{1}{\sqrt{\alpha_1}}z_2\,, \quad \omega_0 = \sqrt{\alpha_1}$$

$$\alpha' = \frac{\alpha_0}{2(\alpha_1 + \alpha_2^2)}\,, \qquad \omega' = \frac{\alpha_0\alpha_2}{2\sqrt{\alpha_1}(\alpha_1 + \alpha_2^2)}$$

$$\mathcal{K} = \frac{1}{8}(3r_{11} + r_{13} + r_{22} + 3r_{24})$$

$$\mathcal{M} = \frac{1}{8}(3r_{21} + r_{23} - r_{12} - 3r_{14})$$

where

$$r_{11} = -\frac{\alpha_1\alpha_2}{\alpha_1^2 + \alpha_2^2}\left(\frac{1}{6} - \frac{\alpha_1^2}{3b^2\delta_{sat}^2}\right)$$

$$r_{13} = \frac{a^2}{b^2\delta_{sat}^2}\cdot\frac{\alpha_1^2\alpha_2}{\alpha_1 + \alpha_2^2}\,, \qquad r_{22} = \frac{a}{b^2\delta_{sat}^2}\cdot\frac{\alpha_1^3}{\alpha_1 + \alpha_2^2}$$

$$r_{24} = \frac{\alpha_1^2}{\alpha_1 + \alpha_2^2}\left(a_3 + \frac{a^3}{3b^2\delta_{sat}^2}\right)$$

$$r_{21} = -\frac{\alpha_2\sqrt{\alpha_1}}{\alpha_2^2 + \alpha_1}\left(\frac{1}{3b^2\delta_{sat}^2}\cdot\frac{\alpha_1^3}{\alpha_2} + \frac{\alpha_2}{6}\right)$$

$$r_{23} = -\frac{a^2}{b^2\delta_{sat}^2}\cdot\frac{\alpha_1^{5/2}}{\alpha_1 + \alpha_2^2}\,, \qquad r_{12} = -\frac{a}{b^2\delta_{sat}^2}\cdot\frac{\alpha_1^{5/2}\alpha_2}{\alpha_1 + \alpha_2^2}$$

$$r_{14} = -\frac{\alpha_1^{3/2}\alpha_2}{\alpha_1 + \alpha_2^2}\left(a_3 + \frac{a^3}{3b^2\delta_{sat}^2}\right)$$

3.3 Results and discussion

Using the ITAE coefficients (12), one can express the previous formulas in terms of the control natural frequency ω_n as follows:

1. Heading angle gain variation k_ψ,

$$\omega_0 = 0{\cdot}756\omega_n$$
$$\alpha' = -0{\cdot}684\omega_n$$
$$\mathcal{K} = 0{\cdot}452\left[3a_3\omega_n^2 + \frac{\omega_n^2}{b^2\delta_{sat}^2} \times (\omega_n^3 + 0{\cdot}5714a\omega_n^2 + 1{\cdot}75a^2\omega_n + a^3 - 1{\cdot}5318\omega_n)\right]$$

2. Yaw rate gain variation k_r,

$$\omega_0 = 1{\cdot}466\omega_n$$
$$\alpha' = -1{\cdot}577(1{\cdot}75\omega_n + a)$$
$$\mathcal{K} = 0{\cdot}0528\left[13{\cdot}8675a_3\omega_n^2 - 0{\cdot}5\omega_n + \frac{2{\cdot}15}{b^2\delta_{sat}^2}\omega_n^2(\omega_n + 2{\cdot}15a)(2{\cdot}15\omega_n^2 + a^2)\right]$$

3. Position error gain variation k_y,

$$\omega_0 = 1{\cdot}466\omega_n$$
$$\alpha' = 0{\cdot}0956\omega_n$$
$$\mathcal{K} = 0{\cdot}0515\left[6{\cdot}45a_3\omega_n^2 - 0{\cdot}875\omega_n + \frac{2{\cdot}15}{b^2\delta_{sat}^2}\omega_n^2(1{\cdot}75\omega_n + a)(2{\cdot}15\omega_n^2 + a^2)\right]$$

In the following, results are presented for the case of k_y variations only. The rest of the cases are qualitatively similar to the ones presented here.[13]

The nonlinear stability coefficient $\mathcal{K}$ is shown in Figs 5 and 6 versus ω_n for different values of the rudder saturation limit δ_{sat} (in radians) and the nonlinear yaw rate coefficient a_3. It is recalled from Section 2.3 that the stability of straight line motion is lost for a value of k_y which is 3·7625 times its nominal value. This is true regardless of the values of the selected natural frequency ω_n. Therefore, in a linear sense, the gain margin is constant and does not distinguish between high or low gain control as evidenced by the magnitude of ω_n. The nonlinear results, however, show a considerable dependence of the robustness properties to parameter variations and unmodeled excitation, on the particular choice of the design parameter ω_n. It appears that low gain control design, i.e. corresponding to relatively low values of ω_n, results in supercritical PAH bifurcations. Small amplitude oscillatory motions are generated after

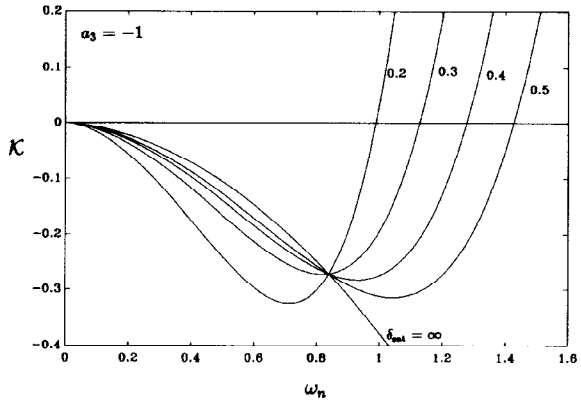

Fig. 5. Variations in k_y: nonlinear coefficient $\mathcal{K}$ versus ω_n for different δ_{sat}.

the nominal equilibrium state loses its stability. Before the critical point is reached, its stability properties are not affected by other nearby attractors in the phase space. The gain margin in such a case would, therefore, represent a true measure of the robustness of the system. Higher values of ω_n, however, inflict a change in the sign of $\mathcal{K}$. This represents a transition from supercritical to subcritical PAH bifurcations, as is schematically shown in Fig. 7. The domain of attraction of the stable nominal equilibrium is becoming increasingly small as the critical point is reached, and its outer bound is given by the unstable limit cycle. Therefore, in such a case it would not be appropriate to rely solely on the critical value C_y as a measure of the robustness of the system. The estimated level of external disturbances must also be taken into consideration since, as shown in Fig. 7, sufficiently large perturbations can throw the vehicle off to an oscillatory steady state even before the critical point is reached. Of course, higher values of ω_n correspond to a wider bandwidth more responsive system, and the final choice will have to be a compromise between speed of response and robustness.

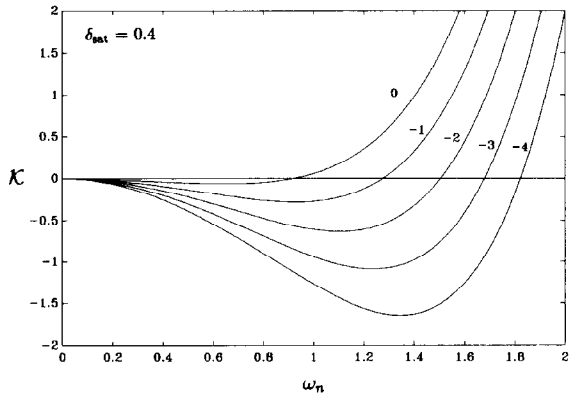

Fig. 6. Variations in k_y: nonlinear coefficient $\mathcal{K}$ versus ω_n for different a_3.

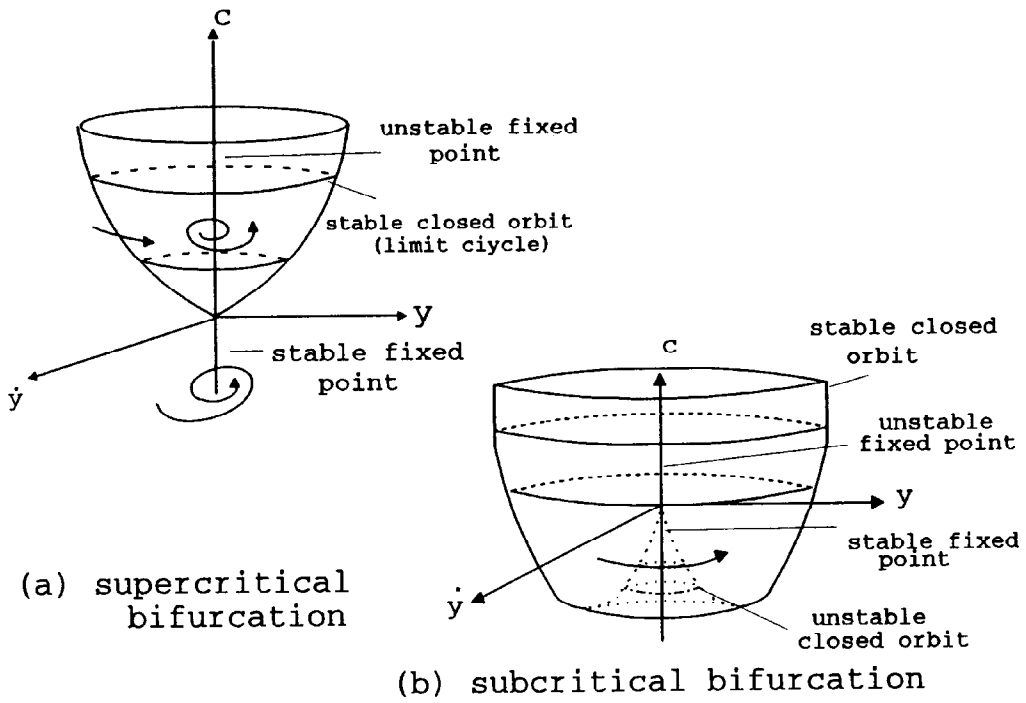

Fig. 7. Supercritical and subcritical Poincaré–Andronov–Hopf bifurcations.

From the results shown in Fig. 5, it can be seen that there exists a value of ω_n where the value of $\mathcal{K}$ is independent of the particular value of δ_{sat}, and is in fact negative. This is a very important property of the system since it can dictate the appropriate range of values of the design parameter ω_n which will ensure the existence of supercritical PAH bifurcations. To explain this property, use the expression for $\mathcal{K}$,

$$\mathcal{K} = 0{\cdot}0515\left[6{\cdot}45a_3\omega_n^2 - 0{\cdot}875\omega_n + \frac{2{\cdot}15}{b^2\delta_{sat}^2}\omega_n^2(1{\cdot}75\omega_n + a)(2{\cdot}15\omega_n^2 + a^2)\right]$$

It can be seen that $\mathcal{K}$ will not depend on δ_{sat} for,

$$\omega_n = -\frac{a}{1{\cdot}75}$$

and using $a = -1{\cdot}47$ it is found that $\omega_n = 0{\cdot}84$ which confirms the results of Fig. 5. The corresponding value of $\mathcal{K}$ is

$$\mathcal{K} = 0{\cdot}0515a(2{\cdot}106a_3a + 0{\cdot}5)$$

which since $a < 0$, $a_3 < 0$, is always negative, thus ensuring supercritical bifurcations. For $a = -1{\cdot}47$, $a_3 = -1$, we find $\mathcal{K} = -0{\cdot}272$, which agrees with the results of the figure.

Due to their practical significance in operations, it is desirable to design the system such that supercritical PAH bifurcations will appear upon initial loss of stability. Transitions between subcritical and supercritical bifurcations occur at precisely those parameter values where the nonlinear stability coefficient, $\mathcal{K}$, crosses zero. For the case of position error gain variation, the condition $\mathcal{K} = 0$ results in,

$$\delta_{sat}^2 = \frac{2{\cdot}15\omega_n(1{\cdot}75\omega_n + a)(2{\cdot}15\omega_n^2 + a^2)}{b^2(0{\cdot}875 - 6{\cdot}45a_3\omega_n)} \tag{47}$$

A plot of (47) is shown in Fig. 8. As expected, the critical value of δ_{sat} is reduced for decreasing ω_n and a_3. Supercritical PAH bifurcations are ensured, for a given vehicle and control law design, for values of δ_{sat} higher than its critical value. Since, as shown by (47), this is directly related to the rudder coefficient b, it can be utilized as a direct design criterion linking the occurrence of supercritical PAH bifurcations to rudder size.

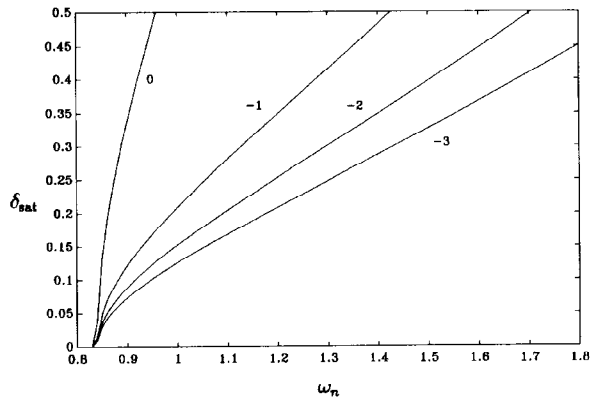

Fig. 8. Critical δ_{sat} versus ω_n for different a_3.

From the results of this section it can also be seen that in the case of unlimited control effort, $\delta_{sat} \to \infty$, all PAH bifurcations are supercritical, $\mathcal{K} < 0$. This is particularly true for the case of yaw rate and position error gain variations. For the heading angle gain variation, the bifurcations would be supercritical only when $a_3 < 0$. If $a_3 = 0$, the cubic coefficient $\mathcal{K}$ would vanish identically, and one would have to resort to higher order expansions to unfold the nature of the bifurcation.[8]

The analytic results confirm the early numerical simulations of Figs 3 and 4. Figure 3 corresponds to a supercritical bifurcation, and convergence to the nominal equilibrium is ensured regardless of the initial conditions used in the integrations. On the other hand, Fig. 4 corresponds to a subcritical bifurcation. Convergence to the stable equilibrium occurs only when the initial conditions are located within the unstable limit cycle which is schematically depicted in Fig. 7. A systematic numerical search can be utilized to determine the actual amplitude of these unstable limit cycles, and is the subject of the next section.

4 PERIODIC SOLUTIONS

4.1 First order approximations

A first order approximation of the limit cycle amplitudes can be obtained from the averaged equation (42). All results presented here correspond to the case of the position error gain variation, k_y. Limit cycles in the original coordinates correspond to the non-trivial stationary solutions of (42), or,

$$R^2 = -\frac{\alpha'\varepsilon}{\mathcal{K}} \tag{48}$$

where for the case of position error gain variation,

$$\varepsilon = C - 3{\cdot}7625$$

Substituting the expressions for α', ε and $\mathcal{K}$ into (48) results in,

$$R^2 = -\frac{1{\cdot}8563b^2\delta_{sat}^2(C - 3{\cdot}7625)}{b^2\delta_{sat}^2(6{\cdot}45a_3\omega_n - 0{\cdot}875) + 2{\cdot}15\omega_n(1{\cdot}75\omega_n + a)(2{\cdot}15\omega_n^2 + a^2)} \tag{49}$$

The lateral deviation y in the original coordinates, can be approximated by (27) which, using the ITAE coefficients becomes,

$$y = \frac{1{\cdot}323}{\omega_n} R\sin(\omega t + \phi) \tag{50}$$

In eqn (50), ϕ is an arbitrary phase angle, whereas the angular frequency ω can be estimated from,

$$\omega = \omega_0 + \omega'\varepsilon = 1{\cdot}466\omega_n + 0{\cdot}1145\omega_n(C - 3{\cdot}7625)$$

Typical results for the first order amplitude expansions y versus C and for different values of ω_n are presented in Fig. 9. Stable attractors are generated for increasing values of C/C_y, whereas unstable attractors exist for decreasing values of C/C_y.

4.2 Numerical simulations

The previous results rely on small amplitude expansions in the vicinity of the bifurcation point and are, therefore, valid only locally in a qualitative sense. In order to gain more insight into the existence of stable and unstable limit cycles, one can perform a systematic numerical search, guided by the theoretical results. A series of numerical integrations was conducted for $\omega_n = 1{\cdot}0$ and $\omega_n = 2{\cdot}0$ in the neighborhood of $C_y = 3{\cdot}7625$, and the results are presented in Fig. 10. For the subcritical PAH bifurcation, it is observed that the resulting unstable limit cycles initially point towards decreasing values of C and then they regain their stability and veer towards increasing values of C, as shown in Fig. 10 by the $\omega_n = 2$ case. Such bifurcation portraits are typical in systems with symmetry.[8] Although such subcritical PAH bifurcations near a degenerate point of the type,

$$\dot{R} = \alpha'\varepsilon R + \mathcal{K}R^3 + \mathcal{L}R^5 \tag{51}$$

such that the unstable limit cycle exhibits a saddle node bifurcation to yield a stable one, may occur for all systems, the analysis is significantly easier for symmetric systems such as the present one. The existence of two limit cycles can occur if the averaged steady state equation,

$$\mathcal{L}R^4 + \mathcal{K}R^2 + \alpha'\varepsilon = 0 \tag{52}$$

admits two real positive solutions in $\mathcal{R}^2$, which depends on the signs of α', ε, the cubic coefficient $\mathcal{K}$, and the quintic coefficient $\mathcal{L}$.

The results of Fig. 10 demonstrate the practical

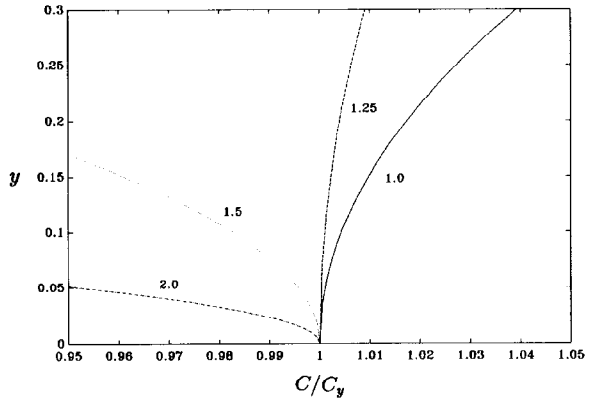

Fig. 9. First order approximations of amplitudes of limit cycles versus C for $a_3 = -1$, $\delta_{sat} = 0{\cdot}4$, and for different values of ω_n.

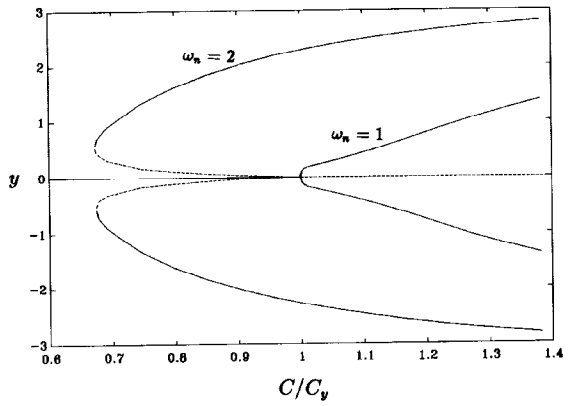

Fig. 10. Numerically computed amplitudes of limit cycles versus C for $a_3 = -1$, $\delta_{sat} = 0{\cdot}4$, and for two values of ω_n.

consequences that are revealed by the nonlinear stability analysis. In the supercritical PAH bifurcation, $\omega_n = 1{\cdot}0$, the linear stability calculations can be considered as reliable. The gain margin, C_y, indeed provides a practical measure of the allowable range of variation of the positional error gain k_y which will maintain the stability of straight line motion. On the other hand, for the subcritical bifurcation, $\omega_n = 2{\cdot}0$, the linear stability calculations should be viewed with caution. The gain margin is not a good indicator of robustness in this case, since it does not guarantee stability of straight line motion under finite disturbances. As Fig. 10 shows, stability is guaranteed provided the gain margin C_y does not exceed approximately 65% of its theoretical value. This becomes progressively smaller as the natural frequency ω_n is increased, which results in higher positive values for $\mathcal{K}$.

5 HYDRODYNAMIC COEFFICIENTS SENSITIVITY

5.1 Loss of stability

Similar studies can be performed in order to establish the sensitivity of the system to changes in the hydrodynamic coefficients a and b. Equation (3) is substituted by,

$$\dot{r} = Car + b\delta \tag{53}$$

Then, the critical value of C, denoted by C_a, is computed by,

$$C_a = \frac{(\alpha_2 + a)\alpha_1 - \alpha_0}{a\alpha_1} = \frac{1{\cdot}28484\omega_n}{a} + 1 \tag{54}$$

Similarly, for variations in the rudder strength coefficient b, one gets

$$\dot{r} = ar + Cb\delta \tag{55}$$

with the characteristic equation,

$$\lambda^3 + [C(\alpha_2 + a) - a]\lambda^2 + C\alpha_1\lambda + C\alpha_0 = 0 \tag{56}$$

The critical value of C is,

$$C_b = \frac{\alpha_0 + a\alpha_1}{\alpha_1(\alpha_2 + a)} = \frac{\omega_n + 2{\cdot}15a}{2{\cdot}15(1{\cdot}75\omega_n + a)} \tag{57}$$

which is the same as C_r for variations in the yaw rate gain k_r, eqn (16). Equation (57) is valid for as long as all the coefficients of (56) are positive, i.e.

$$C_b \geq 0\,, \quad C_b(\alpha_2 + a) - a \geq 0$$

The system is unstable for all values of the natural frequency if C is less than zero. When the natural frequency is in the range $0 \leq \omega_n \leq |a/1{\cdot}75|$, the stability changes from stable to unstable with an increase in C, for positive C. In the range $\omega_n \geq |2{\cdot}15a|$, stability changes from unstable to stable as C crosses the critical point again for positive C. In both cases, a pair of complex conjugate eigenvalues crosses the imaginary axis. Stability is also lost when C becomes negative, but this is associated with one real eigenvalue crossing zero. In this work the authors have concentrated on the $C > 0$ case since, in applications, it is unlikely that a change in the sign of b will occur without the designer's knowledge.

5.2 Hopf bifurcations

Using similar center manifold reduction and integral averaging techniques, the following results are obtained:

1. Variation in a,

$$\omega_0 = 1{\cdot}466\omega_n$$

$$\alpha' = -0{\cdot}454a$$

$$27{\cdot}75\mathcal{K} = \frac{1}{b^2\delta_{sat}^2} \times \left[6{\cdot}7779\omega_n^5 + \left(\frac{1}{1{\cdot}4662\omega_n} + 14{\cdot}5725\omega_n^4\right) \times (-\omega_n^6 + (4{\cdot}3\omega_n^5 - 1)(1{\cdot}75\omega_n + a))\right] + \frac{0{\cdot}7166}{b^2\delta_{sat}^2}\omega_n^2(1{\cdot}884\omega_n + 1{\cdot}4663a)^3 - 0{\cdot}7331\omega_n + 6{\cdot}7779a_3\omega_n^2$$

2. Variation in b,

$$\omega_0 = \omega_n\sqrt{\frac{\omega_n + 2{\cdot}15a}{1{\cdot}75\omega_n + a}}$$

$$\alpha' = -\frac{(\omega_n + 2{\cdot}15a)(1{\cdot}75\omega_n + a)}{2{\cdot}38\omega_n + 4{\cdot}52a}$$

$$\frac{8(6{\cdot}3725\omega_n^2 + a\omega_n + 4{\cdot}6225a)}{\omega_n^2}\mathcal{K} = 2{\cdot}15a^3\omega_n\frac{(\omega_n + 2{\cdot}15a)^2}{1{\cdot}75\omega_n + a} - 1.075(\omega_n + 2{\cdot}15a) + \frac{9{\cdot}9384\omega_n^2}{b^2\delta_{sat}^2}[2{\cdot}15\omega_n^3(\omega_n + 2{\cdot}15a)^2 + a(1{\cdot}75\omega_n + a)(1 + 4{\cdot}6225a^2\omega_n)]$$

Results are presented by Oral[13] and they are qualitatively similar to the gain variations studied previously. Namely, supercritical PAH bifurcations occur for values of ω_n up to a critical value, with the subsequent evolution of subcritical bifurcations.

5.3 Sensitivity study

Of interest in applications is a sensitivity study of the control system to inaccuracies in the modeling of the hydrodynamic coefficients in (1) and (2). These equations were utilized to produce the approximate first order model (3) by substituting,

$$a = -\frac{1}{T}, \qquad b = \frac{K}{T} \tag{58}$$

where K and T are Nomoto's coefficients,

$$T = \frac{(Y_{\dot v} - m)(N_r - mx_G) + (N_{\dot r} - I_z)Y_v}{Y_v(N_r - mx_G) - N_v(Y_r - m)} - \frac{(Y_{\dot r} - mx_G)N_v + (N_{\dot v} - mx_G)(Y_r - m)}{Y_v(N_r - mx_G) - N_v(Y_r - m)} - \frac{(N_{\dot v} - mx_G)Y_\delta - (Y_{\dot v} - m)N_\delta}{N_v Y_\delta - Y_v N_\delta} \tag{59}$$

$$K = \frac{N_v Y_\delta - Y_v N_\delta}{Y_v(N_r - mx_G) - N_v(Y_r - m)} \tag{60}$$

Typical results are presented in Fig. 11 where the ratio a/a_{nom} versus x/x_{nom} is plotted where x represents any one of the four main hydrodynamic derivatives Y_v, $Y_{\dot v}$, N_r, and $N_{\dot r}$. The results for b are similar. It can be seen that the most significant inaccuracies in the determination of a and b will most likely arise from inaccuracies in the estimates of the yaw damping N_r and the yaw added mass $N_{\dot r}$, while sway velocity coefficients do not play a significant role. Although this is especially true for the NPS vehicle which has a particularly small side slip during turning, the results should be considered representative for most marine vehicles of conventional hull shapes.

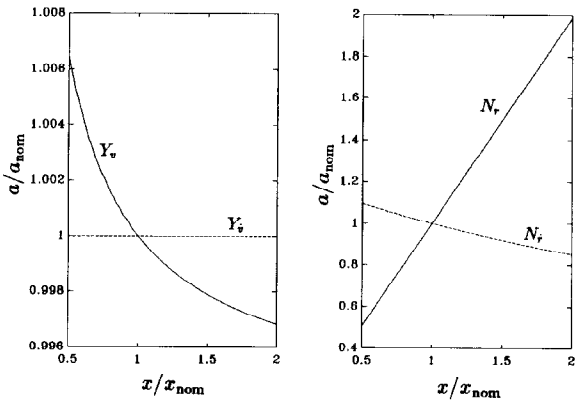

Fig. 11. Typical hydrodynamic coefficients sensitivity results.

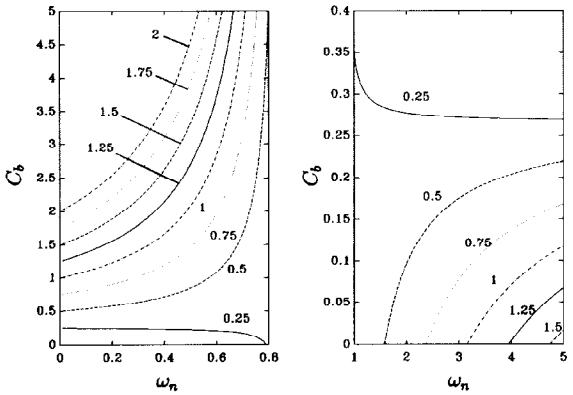

Fig. 12. Stability contours (C_b, ω_n) with C_a as a parameter.

In general, errors in the estimate of one or more hydrodynamic coefficients will inflict changes in both coefficients a and b. Therefore, one is forced to consider a system of the form,

$$\dot r = C_a a r + C_b b \delta \tag{61}$$

The characteristic equation based on (61) is,

$$\lambda^3 + [C_b(\alpha_2 + a) - C_a a]\lambda^2 + C_b\alpha_1\lambda + C_b\alpha_0 = 0 \tag{62}$$

Loss of stability of (62) occurs at the critical point,

$$C_b(\alpha_2 + a) - C_a a = \frac{\alpha_0}{\alpha_1} \tag{63}$$

Equation (63), assuming that all coefficients in (62) are positive, determines the stability contours of the system for combined variations in a and b. Typical results are presented in Fig. 12, where the regions of stability and instability are similar to those shown in Fig. 2. Along the critical curves shown in the figure, the system undergoes a PAH bifurcation to periodic solutions, which can be analyzed using the same techniques as before; the results are qualitatively similar to the b variations studied previously.

6 CONCLUDING REMARKS

An analytic investigation of the nonlinear dynamic response of a path keeping control law for marine vehicles has been presented. Particular emphasis was placed on a critical analysis of the control system gain margins, as they are frequently used to characterize the robustness to parameter variations and modeling errors. Bifurcation theory techniques were utilized in order to assess the behavior of the system upon initial loss of stability of straight line motion. The principal bifurcation parameters were the control natural frequency, control saturation level, system hydrodynamic parameters, and control system gains. The main conclusions of this work can be summarized as follows:

1. There exists a critical point for a certain combination of system gains and system parameters for the stability of straight line motion. The loss of stability occurs generically in the form of Poincaré–Andronov–Hopf bifurcations. As the parameter crosses its critical value, a family of periodic orbits, self-sustained oscillations, develops. Center manifold reduction and integral averaging techniques were used in order to establish the direction of the bifurcation and the stability of the resulting periodic solutions.
2. A high closed-loop natural frequency is desirable for wider system bandwidth and faster response. However, it was shown that subcritical bifurcations will develop for sufficiently high natural frequencies. In such a case, the periodic solutions develop with what appears to be a discontinuous increase in the amplitude of oscillations. Furthermore, the stability of straight line motion before the critical point is reached can not be guaranteed for finite disturbances.
3. Supercritical bifurcations are encountered for sufficiently low values of the control natural frequency. In this benign loss of stability, the resulting periodic solutions are continuous single-valued functions of the parameter distance from its critical value. Global asymptotic stability appears to be guaranteed for straight line motion prior to loss of stability, for arbitrary levels of initial conditions. The final choice for the control natural frequency must be a compromise among speed of response, path accuracy, noise rejection, and robustness as measured by the nonlinear stability coefficient K.
4. The occurrence of subcritical bifurcations is delayed by increasing the available control effort and/or increasing the speed loss during turning. Both of these options require higher energy consumption and are, therefore, not practical. Instead, a comprehensive examination of the nature of the bifurcation must be undertaken in order to suggest viable alternatives.
5. The concept of gain margin should be viewed only in conjunction with the nonlinear properties of the system. It can safely represent a measure of robustness for this system only in the case of a supercritical bifurcation to periodic solutions. For this reason, transitions from supercritical to subcritical PAH bifurcations should be studied during control system design, particularly if significant modeling inaccuracies or deviations from a nominal operating condition are expected.

ACKNOWLEDGEMENT

The authors would like to recognize the financial support of the Naval Postgraduate School Direct Research Fund.

REFERENCES

1. Parsons, M. G. & Cuong, H. T., Optimal stochastic path control of surface ships in shallow water. Office of Naval Research Report No. ONR–CR–215–249–2F, 1977.
2. Parsons, M. G. & Cuong, H. T., Adaptive path control of surface ships in restricted waters. Department of Naval Architecture and Marine Engineering, Report No. 211, The University of Michigan, Ann Arbor, 1980.
3. Parsons, M. G. & Cuong, H. T., Surface ship path control using multivariable integral control. Department of Naval Architecture and Marine Engineering, Report No. 233, The University of Michigan, Ann Arbor, 1981.
4. Healey, A. J., Model-based maneuvering controls for autonomous underwater vehicles. *Journal of Dynamic Systems, Measurement, and Control*, Transactions of the ASME, **114** (1992) 614–22.
5. Papoulias, F. A. & Healey, A. J., Path control of surface ships using sliding modes. *Journal of Ship Research*, **36** (1992) 2.
6. Yoerger, D. R. & Slotine, J.-J. E., Robust trajectory control of underwater vehicles. *IEEE Journal of Oceanic Engineering*, **10** (1985) 4.
7. Papoulias, F. A., Bifurcation analysis of line of sight vehicle guidance using sliding modes. *International Journal of Bifurcation and Chaos*, **1** (1991) 4.
8. Guckenheimer, J. & Holmes, P., *Nonlinear Oscillations, Dynamical Systems, and Bifurcations of Vector Fields*. Applied Mathematical Sciences 42, Springer, New York, 1983.
9. Chow, S.-N. & Mallet-Paret, J., Integral averaging and bifurcation. *Journal of Differential Equations*, **26** (1977) 112–59.
10. Friedland, B., *Control System Design: An Introduction to State–Space Methods*. McGraw Hill, New York, 1986.
11. Bahrke, F., On-line identification of the speed, steering and diving response parameters of an autonomous underwater vehicle from experimental data. Mechanical Engineer's Thesis, Naval Postgraduate School, Monterey, California, 1992.
12. Crane, C. L., Eda, H., & Landsburg, A., Controllability. In *Principles of Naval Architecture*, Ch. IX, ed. E. V. Lewis. The Society of Naval Architects and Marine Engineers, New York, 1989.
13. Oral, Z. O., Hopf bifurcations in path control of marine vehicles. MS thesis, Department of Mechanical Engineering, Naval Postgraduate School, Monterey, California, 1993.
14. Hassard, B. & Wan, Y.H., Bifurcation formulae derived from center manifold theory. *Journal of Mathematical Analysis and Applications*, **63** (1978) 297–312.